(Preprint) AAS 23-142

SAFETY IN FORCED MOTION GUIDANCE FOR PROXIMITY OPERATIONS BASED ON RELATIVE ORBITAL ELEMENTS

Giacomo Borelli*, Gabriella Gaias†, and Camilla Colombo‡

Autonomous spacecraft proximity operations represent a key enabler for future mission architectures such as in-orbit servicing, active debris removal, objects' inspection, and in-orbit assembly. This work addresses safety concepts for the relative trajectory guidance design applicable to challenging proximity operations in the close-range domain. The relative orbital elements framework is used to formulate safety checks which improve the trajectory robustness in case of chaser's malfunctions or loss of control. Particularly, concepts of passive abort safety and active collision safety are applied to the trajectory design to maintain the chaser outside keep-out-zones. These definitions are included within a guidance algorithm that exploits sequential convex programming to efficiently solve the fixed final time safety constrained close-range rendezvous problem. Test cases of reconfiguration between stable relative orbits and synchronisation to a rotating hold point are presented, highlighting the advantages in the use of these new safety concepts, in terms of safety, trajectory insight and formulation efficiency.

INTRODUCTION

Proximity operations play an important role in future mission architectures in the On-Orbit Servicing, Assembly and Manufacturing (OSAM) domain. A paradigm shift between monolithic one-use assets towards OSAM activities in space is recognised as both profitable and efficient for the future space economy by the global space community. Despite a rich heritage of Rendezvous and Proximity Operations (RPOs) to cooperative targets, advances in the design of operations to uncooperative and non-collaborative targets are instrumental for a systematic implementation of autonomous RPOs within OSAM activities in the future. One of the key enablers for autonomous proximity operations to uncooperative and non-collaborative targets is flight safety. In fact, any anomaly with respect to the nominal profile or any contingency at spacecraft level will cause the triggering of safety measures, ultimately leading to chaser s/c in safe mode, thus potentially endangering the platforms and/or the completion of the mission. Such situations are not unknown to past missions. In the JAXA robotic demonstration mission ETS-VII,[1] anomalies during an experiment caused the spacecraft to abort operations and position itself at 2.5 km distance from the target while investigating the issue. In 2005 during DART mission, the chaser unexpectedly used all the on-board propellant and during the retirement manoeuvres a collision with the target was detected.[2] More recently in early 2022 ELSA-d demonstration failures in the thrusters' assembly

*Ph.D. Candidate, Department of Aerospace Science and Technology, Politecnico di Milano, Via La Masa, 34, 20156, Milano - Italy. giacomo.borelli@polimi.it

†Assistant Professor, Department of Aerospace Science and Technology, Politecnico di Milano, Via La Masa, 34, 20156, Milano - Italy. gabriella.gaias@polimi.it

‡Associate Professor, Department of Aerospace Science and Technology, Politecnico di Milano, Via La Masa, 34, 20156, Milano - Italy. camilla.colombo@polimi.it

caused the chaser to move away at a safe distance from the target and a consequent re-assessment and re-planning of rendezvous and docking demonstration operations.[3]

In this work trajectory safety is studied and included in a novel guidance strategy for the proximity operations scenarios. The objective of this work is twofold: (1) to improve the proximity safety formulations through an understanding and description of the relative dynamics, (2) to develop a computationally efficient safe guidance solution to enable autonomous operations. Autonomy and flight safety are strongly correlated in proximity operations, since the inherent safe planning of operations will allow a less strict requirement on ground-support.

The general approach to guarantee safety in relative trajectory guidance is to define a geometric Keep Out Zone (KOZ) around the target object. The chaser trajectory is then defined ensuring the avoidance of the KOZ along its path. The safety path conditions can then be readily included as constraints to the guidance problem formulated as a Nonlinear Programming Problem (NLP).[4] By assuming the KOZ to be a concave surface, the resulting constraint formulation lead to non-convex NLP. Reformulation of concave regions, and in general non-convex constraints, with simplification or relaxations of them but formulated with in a convex formulation can lead to simpler optimisation problems, such as Linear Programming (LP)[5,6] or second order Cone Programming problems (SOCP).[7–9] Strategies such as Sliding Mode Control (SMC) and Artificial Potential Functions (APF) are also explored in literature to impose the avoidance of regions through repulsive functions in a feedback fashion.[10–12] Another useful formulation of flight safety in proximity operations is Passive Abort Safety (PAS) thanks to its robustness against major system's failures during the mission. In fact, PAS guarantees collision avoidance with the target in the case of complete loss of controllability of the chaser platform. Specifically, the concept of E/I separation to impose PAS was demonstrated in flight during the GRACE formation flying mission[13] and far-range rendezvous missions such as PRISMA[14] and AVANTI.[15,16] This concept can be implemented in a straightforward fashion by exploiting the Relative Orbital Elements (ROE) parametrization of the relative dynamics.[17,18] E/I separation guarantees a minimum separation in a plane orthogonal to the target orbital velocity in near-circular orbits which leads to collision avoidance even in the case of total loss of control of the chaser. The method has been extensively employed in studies of uncooperative far-range rendezvous[19,20] and inspection phases.[21,22]

In this work the formulation of trajectory safety in proximity operations are introduced exploiting the ROE framework. The contribution of this paper is the definition of trajectory safety concepts similar to E/I vector separation applicable to the demanding scenarios of forced motion in close-range, in the range of 10-100 meters of separation from the target. These formulations are introduced to guarantee different levels of safety considered, such as passive abort safety or active collision safety after a collision avoidance policy actuation. Possible applications comprehend formation reconfiguration, approach, and forced motion synchronisation in presence of the uncooperative and non-collaborative target. The novel definitions of passive abort safety and active collision safety in function of ROEs are included in a guidance scheme solved through a Sequential Convex Programming (SCP) approach,[23–25] particularly fit to autonomous on-board guidance implementations. The guidance method is described and the results of two representative test cases are analysed. The paper is organized in the following manner: after an introduction on the relative dynamics models and ROE parametrisation employed, the definitions and novel formulations of safety conditions for proximity operations in function of ROEs are described. Then, the transcription and solution method of the guidance problem formulated as a constrained fixed time optimal control is presented. Two test cases are then shown to demonstrate the efficiency of the guidance

solution proposed and the improvement on the trajectory safety features. Lastly, some conclusions are drawn.

RELATIVE MOTION MODEL

The relative dynamics of two objects flying in close proximity can be modelled with a linear system. In this work the relative state is parametrized in quasi-nonsingular ROEs and the satellites are assumed to be on near-circular orbits. Accordingly, the ROEs represent the integrals of the relative motions in the Keplerian hypothesis. The dimensionless ROE state vector is expressed in function of chaser's and target's Keplerian elements as follows:[17]

$$\delta\boldsymbol{\alpha} = \begin{pmatrix} \delta a \\ \delta\lambda \\ \delta e_x \\ \delta e_y \\ \delta i_x \\ \delta i_y \end{pmatrix} = \begin{pmatrix} (a_c - a_t)/a_c \\ u_c - u_t + (\Omega_c - \Omega_t)\cos in_c \\ e_c\cos\omega_c - e_t\cos\omega_t \\ e_c\sin\omega_c - e_t\sin\omega_t \\ in_c - in_t \\ (\Omega_c - \Omega_t)\sin in_c \end{pmatrix} \tag{1}$$

The quantities $(\cdot)_c$ and $(\cdot)_t$ are the Keplerian elements of the chaser orbit and target orbit respectively. Specifically, a is the semi-major axis, e the eccentricity, in the inclination, Ω the right ascension of the ascending node, ω the argument of periapsis and u the mean argument of latitude. By expressing the ROE vector time derivative in function of Keplerian elements rates and by expanding through a first order Taylor series about the target orbit, the dynamics of the ROE state can be expressed in linear form as follows:

$$\dot{\delta\boldsymbol{\alpha}} = \mathrm{A}\delta\boldsymbol{\alpha} + \mathrm{B(t)}\mathbf{u} \tag{2}$$

where the plant matrix A considering only the Keplerian dynamics and the time-varying control input matrix $\mathrm{B(t)}$ result in:

$$\mathrm{A} = \begin{bmatrix} 0 & 0 & 0 & 0 & 0 & 0 \\ -L_n & 0 & 0 & 0 & 0 & 0 \\ 0 & 0 & 0 & 0 & 0 & 0 \\ 0 & 0 & 0 & 0 & 0 & 0 \\ 0 & 0 & 0 & 0 & 0 & 0 \\ 0 & 0 & 0 & 0 & 0 & 0 \end{bmatrix} \quad \mathrm{B} = \frac{1}{na}\begin{bmatrix} 0 & 2 & 0 \\ -2 & 0 & 0 \\ \sin u & 2\cos u & 0 \\ -\cos u & 2\sin u & 0 \\ 0 & 0 & \cos u \\ 0 & 0 & \sin u \end{bmatrix} \tag{3}$$

$$\text{with} \quad L_n = -\frac{3}{2}n \qquad u = nt + u_0$$

The quantity n represents the orbit mean motion which, under Keplerian assumption, correlates linearly with the argument of latitude u, which is a function of time. The quantity u_0 is the argument of latitude at time $t = 0$. The resulting linear dynamics are obtained considering only the Keplerian accelerations acting on the chaser and target orbits. Therefore the validity is retained only when non-Keplerian perturbing effects are negligible. In particular, in the near-Earth environment, the effects of Earth's oblatness and atmosphere drag need to be considered when longer time intervals are studied. The solution of the linear dynamics of Equation 2 can be expressed through the State Transition Matrix (STM) as follows:[18]

$$\delta\boldsymbol{\alpha}(t) = \Phi(t_0, t)\delta\boldsymbol{\alpha}_0 + \int_{t_0}^{t} \Phi(t_0, \tau)\mathrm{B}(\tau)\boldsymbol{u}(\tau)d\tau \tag{4}$$

where $\Phi(t_i, t_{i+1})$ represents the STM from time t_i to t_{i+1}, and is expressed as:

$$\Phi(t_0, t) = \begin{bmatrix} 1 & 0 & 0 & 0 & 0 & 0 \\ -L_n(t-t_0) & 1 & 0 & 0 & 0 & 0 \\ 0 & 0 & 1 & 0 & 0 & 0 \\ 0 & 0 & 0 & 1 & 0 & 0 \\ 0 & 0 & 0 & 0 & 1 & 0 \\ 0 & 0 & 0 & 0 & 0 & 1 \end{bmatrix} \tag{5}$$

In the cases where the input acceleration vector $\mathbf{u}$ is constant over a time interval $[t_0, t]$, Equation 4 can be expressed as:

$$\delta\boldsymbol{\alpha}(t) = \Phi(t_0, t)\delta\boldsymbol{\alpha} + \Psi(t_0, t)\mathbf{u} \tag{6}$$

where the matrix $\Psi(t_0, t)$ is the solution of the definite integral of Equation 4 between t_0 and t. A Lyapunov transformation defined as mapping between dimensional ROEs $a\delta\boldsymbol{\alpha}$ and Cartesian coordinates in the Radial Tangential Normal (RTN) frame is reported as follows:[18]

$$a\delta\boldsymbol{\alpha} = \Gamma(t)\delta\boldsymbol{x} \tag{7}$$

$$\Gamma(t) = \begin{bmatrix} 1 & 0 & -\cos(nt) & -\sin(nt) & 0 & 0 \\ 0 & 1 & 2\sin(nt) & -2\cos(nt) & 0 & 0 \\ 0 & 0 & 0 & 0 & \sin(nt) & \cos(nt) \\ 0 & 0 & n\sin(nt) & -n\cos(nt) & 0 & 0 \\ -(3n)/2 & 0 & 2n\cos(nt) & 2n\sin(nt) & 0 & 0 \\ 0 & 0 & 0 & 0 & n\cos(nt) & n\sin(nt) \end{bmatrix} \tag{8}$$

This mapping is accurate for small separation between the spacecraft and under Keplerian dynamics. The inclusion of non-Keplerian perturbation effects and higher order effects is required where a large separation or highly perturbed environments are encountered.

TRAJECTORY SAFETY FORMULATIONS

To guarantee smooth and robust close proximity operations, trajectory safety is to be considered a key feature for the proximity GNC strategies. Indeed, during operations around uncooperative and non-collaborative targets the inclusion of safety within the trajectory design is of utmost importance. In this section the novel safety concepts developed in this work are introduced and described. The following different safety formulations will enforce the avoidance of a geometrical KOZ during the nominal and non-nominal flight conditions around the non-collaborative and uncooperative target. In the latter scenarios, the fulfilment of safety measures during the proximity operations solely depends on the design of operations of chaser platform, being the target completely inactive.

The following definitions of trajectory safety at time t_i will be used throughout this paper:

- **Point-Wise Safety (PWS)**: Chaser's trajectory at time t_i is said to be PWS safe if it is outside a geometrical KOZ defined around the target only at the time instant t_i.
- **Passive Abort Safety (PAS)**: Chaser's trajectory at t_i is said to be PAS safe for a time interval ΔT if it is outside a geometrical KOZ around the target at time t_i, and it will remain outside such KOZ also after a ΔT time interval of uncontrolled flight starting at t_i.

- **Active Collision Safety (ACS)** : Chaser's trajectory at t_i is said to be ACS safe if at time t_i is outside a geometrical KOZ around the target, and it will remain outside such KOZ even for a $\Delta T_{ACS} + \Delta T$ time interval after t_i. The intervals ΔT_{ACS} and ΔT are respectively the controlled collision avoidance portion and the uncontrolled portion of the trajectory after t_i.

The definition of PAS is used to extend the safety condition in the future in the case where any contingency or failure causes the complete loss of controllability of the chaser platform. While, the definition of ACS guarantees safety in situations where the chaser detects some anomalies/failures that endanger the completion of the approach operations but retains the capability of the platform to perform collision avoidance manoeuvres.

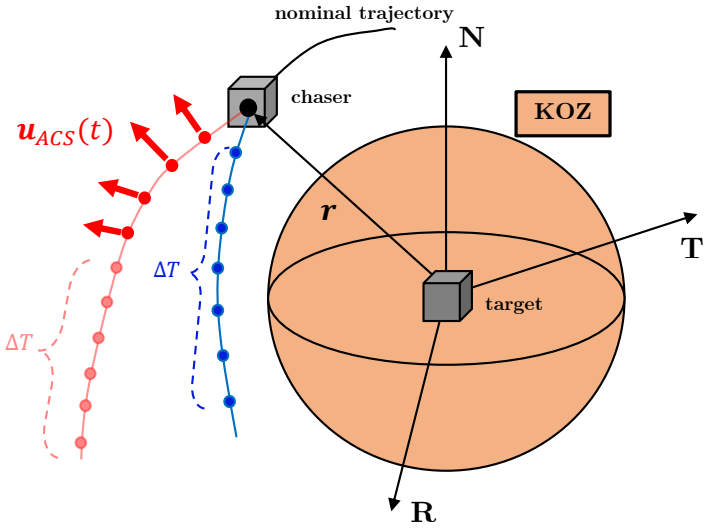

Figure 1: Schematic representation of the safety concepts in the RTN frame centred on the target. The chaser is on the nominal trajectory depicted in black. At time t_i, PAS is evaluated on the uncontrolled trajectory branch in blue. If required, ACS is enforced on the (partly) actively controlled branch in red.

In proximity trajectory design PWS is often treated considering a KOZ around the regions to be avoided and it is expressed with a quadratic form as in Equation 9.

$$\delta \boldsymbol{x}^{\mathrm{T}}(t_i) \mathrm{Q} \delta \boldsymbol{x}(t_i) \geq R_{KOZ} \tag{9}$$

The vectors $\delta \mathbf{x}$ are the cartesian position vector in RTN, and the matrix Q and scalar R_{KOZ} denote constants that govern the geometry of the KOZ. This formulation is extensively used in trajectory design problems thanks its simplicity and its immediate interpretation. Often the concave avoidance region is formulated through a convex relaxation to simplify the inclusion within the guidance problems and aid the solution efficiency.[5–9] Nonetheless, Equation 9 can only guarantee safety at the enforced times t_i along the nominal trajectory. On the contrary, PAS strengthens the PWS conditions by extending the safety in the future evolution of an uncontrolled trajectory stemming from the nominal trajectory at the considered times, see Figure 1. In this framework, a straightforward implementation of PAS would be to include an additional set of instants for the uncontrolled trajectory, such that the safety checks of Equation 9 are imposed on both nominal and augmented time instants.

Despite the apparent simplicity of this approach, the size of the problem can quickly become prohibitive whenever the PAS is required for long time intervals and/or for many instants of a trajectory. An alternative concept of PAS has been implemented in proximity flight at larger separations based on relative eccentricity and relative inclination vectors separation.[13,15,16] The great advantage of these strategy is that PAS can be expressed and guaranteed as a single condition on the ROE state at time t_i without the need of enforcing additional safety conditions in future states of the uncontrolled trajectory evolution. Accordingly, this PAS formulation provides a simple and computationally light solution to support guidance and Fault Detection Isolation and Recovery (FDIR) algorithms for autonomous operations, once selected a specific phasing of the relative eccentricity and inclination vectors. Briefly, E/I separation considers the minimum inter-satellite distance on the Radial Normal (RN) plane of relative trajectory characterised by parallel or anti-parallel relative eccentricity and inclination vectors. Such minimum distance is expressed by the following Equation.

$$\min_{u\in[0,2\pi]} \quad \sqrt{\delta x_R^2(t) + \delta x_N^2(t)} = \min\{\|\delta \boldsymbol{i}\|, \|\delta \boldsymbol{e}\| - |\delta a|\} \tag{10}$$

An extension of this concept is developed in this work to employ a similar approach in close proximity scenarios, including forced motion phases. In the close-range, in fact, the relative trajectory generally is subject to more complex boundary constraints, not compatible with a simple (anti-) parallel phasing of the relative eccentricity/inclination vectors. Examples are forced fly-around or reconfigurations to different relative orbits, where maintaining a E/I vector separation along the whole trajectory is not possible. The relaxation of the parallel or anti-parallel conditions for the relative eccentricity $\delta \boldsymbol{e}$ and relative inclination $\delta \boldsymbol{i}$ is required. The subsequent treatment of PAS safety extend the concept of minimum separations between the chaser and the target by studying the natural motion evolution in RTN described by a ROE state. The subsequent definition of minimum separations in function of the ROE state are done recalling the final aim of including such safety checks as constraint in a guidance algorithm.

Firstly a treatment of PAS by guaranteeing a minimum separation in the RN plane is presented. From the Lyapunov transformation between ROE and cartesian RTN states of Equation 8, the radial and normal relative position vector components can be expressed in function of ROEs as follows:

$$\begin{cases} \delta x_R/a = \delta a - \delta e \sin(u-\varphi) \\ \delta x_N/a = \delta i \cos(u-\theta) \end{cases} \tag{11}$$

where the angular variables φ (argument of perigee of the relative orbit) and θ (ascending node of the relative orbit) represent the phasing of the relative eccentricity and inclination vectors and can be written in function of the ROE state as:

$$\tan\varphi = \frac{\delta e_y}{\delta e_x} \qquad \tan\theta = \frac{\delta i_y}{\delta i_x} \tag{12}$$

Geometrically, the RN trajectory related to a ROE state for different argument of latitudes, i.e. times, is a rotated and translated ellipse $\mathcal{E}_{RN}$. The geometrical quantities of the rotated ellipse, shown in Figure 2a, can be expressed analytically in function of the ROE state as follows:

$$\begin{cases} a_{RN} = \left[\frac{1}{2}\left(\delta e^2 + \delta i^2 + \sqrt{\delta e^4 + \delta i^4 - 2\delta e^2 \delta i^2 \cos\left(2(\pi+\theta-\varphi)\right)}\right)\right]^{0.5} \\ b_{RN} = \left[\frac{1}{2}\left(\delta e^2 + \delta i^2 - \sqrt{\delta e^4 + \delta i^4 - 2\delta e^2 \delta i^2 \cos\left(2(\pi+\theta-\varphi)\right)}\right)\right]^{0.5} \\ \cos^2\gamma = \frac{1}{2} + \frac{\frac{1}{2}(\delta e^2 - \delta i^2)}{\sqrt{\delta e^4 + \delta i^4 - 2\delta e^2 \delta i^2 \cos(2(\pi+\theta-\varphi))}} \end{cases} \tag{13}$$

where a_{RN} is the ellipse's semi-major axis, b_{RN} the semi-minor axis γ and the inclination of the former with respect to the R axis. A relative semi-major axis difference δa is a translation of the projected ellipse $\mathcal{E}_{RN}$ on the R axis. Introducing the E/I condition translates in $\varphi = \theta + k\pi$ and for the situation where the RN ellipse has no rotation with respect the radial direction R. Moreover, in this case the distance with respect to the origin of the RN plane is trivially obtained. On the other hand, the solution of Equation 10 to find the minimum distance between the ellipse $\mathcal{E}_{RN}$ and the origin of the RN plane without introducing the E/I assumption reduces to solving a quartic equation to find the argument of latitude u of minimum separation.[16] In this work a simplification of the minimum distance is introduced by defining a closed polytope included within the ellipse shape resulting from the projection of the trajectory of ROE state onto the RN plane.

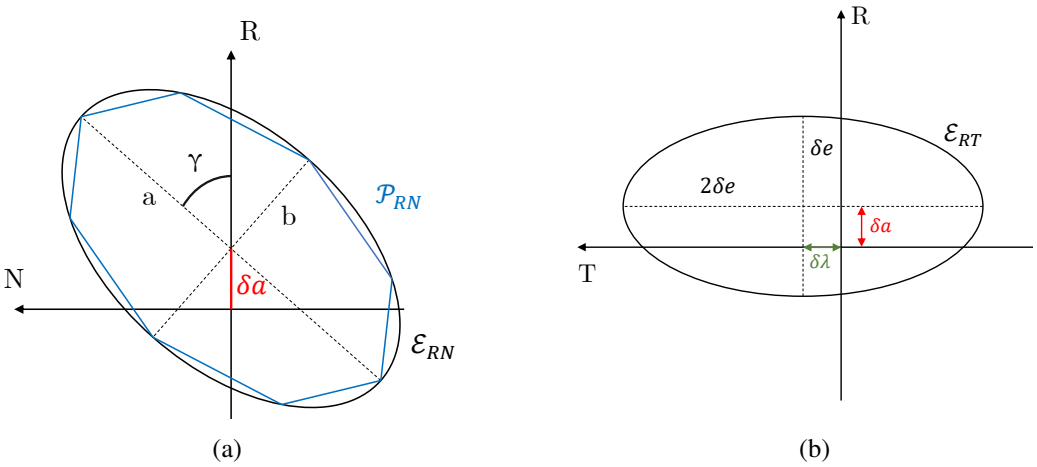

Figure 2: Geometrical projection of the relative trajectory correspondent to a ROE state $\delta\boldsymbol{\alpha}$ for varying argument of latitude u. Projection in the RN plane (a) and RT plane (b) are shown.

The minimum distance between a KOZ around the origin of the RN frame from a polytope $\mathcal{P}_{RN}$ enclosed in the translated and rotated ellipse can be expressed explicitly using inequality conditions. In this work it is considered a polytope generated with two lines per ellipse's quadrant as in Figure 2a. Accordingly, the two conditions to be enforced are:

$$\begin{cases} \left(|\delta a|\sin\gamma - m_1|\delta a|\cos\gamma - q_1\right)\left(1+m_1^2\right)^{-0.5} + R_{KOZ,RN} \leq 0 \\ \left(|\delta a|\sin\gamma - m_2|\delta a|\cos\gamma - q_2\right)\left(1+m_2^2\right)^{-0.5} + R_{KOZ,RN} \leq 0 \end{cases} \tag{14}$$

with

$$\begin{cases} m_1 = \left(\frac{\sqrt{1-k^2}-1}{k}\right)\left(\frac{\delta e^2+\delta i^2-\sqrt{\delta e^4+\delta i^4-2\delta e^2\delta i^2\cos(2\varphi-2\theta)}}{\delta e^2+\delta i^2+\sqrt{\delta e^4+\delta i^4-2\delta e^2\delta i^2\cos(2\varphi-2\theta)}}\right)^{0.5} \\ m_2 = \left(\frac{\sqrt{1-k^2}}{k-1}\right)\left(\frac{\delta e^2+\delta i^2-\sqrt{\delta e^4+\delta i^4-2\delta e^2\delta i^2\cos(2\varphi-2\theta)}}{\delta e^2+\delta i^2+\sqrt{\delta e^4+\delta i^4-2\delta e^2\delta i^2\cos(2\varphi-2\theta)}}\right)^{0.5} \\ q_1 = \left(\frac{\delta e^2}{2}+\frac{\delta i^2}{2}-\frac{\sqrt{\delta e^4+\delta i^4-2\delta e^2\delta i^2\cos(2\varphi-2\theta)}}{2}\right)^{0.5} \\ q_2 = -\left(\frac{\sqrt{1-k^2}}{k-1}\right)\left(\frac{\delta e^2}{2}+\frac{\delta i^2}{2}-\frac{\sqrt{\delta e^4+\delta i^4-2\delta e^2\delta i^2\cos(2\varphi-2\theta)}}{2}\right)^{0.5} \end{cases} \tag{15}$$

where $R_{KOZ,RN}$ is the radius of the spherical KOZ around the origin of the RTN frame. The parameter k in this specific case governs the point on which polytope's lines connects within the ellipse. This definition can be extended to polytopes with more sides, hence more lines per quadrant in a straightforward fashion. In these cases, the safety conditions expressed in Equation 14 will be the of same number as the polytope lines. It is worth remarking that the geometrical conditions of minimum distance formulated are valid if the origin of the RN plane, hence the target, is within the ellipse $\mathcal{E}_{RN}$. The cases where the target is outside of $\mathcal{E}_{RN}$ correspond to cases where there is a large translation of the ellipse on the radial direction induced by δa with respect to the fundamental sizes of the ellipse. In other words the introduced condition limits the possible δa drift of the ROE state in function of the magnitudes of the relative eccentricity and inclination vectors, which determine the fundamental ellipse size as detailed in Equation 13.

The second definition of ROE-based minimum separation convenient for safety formulation considers the projection of the relative trajectory on the Radial Transversal (RT) plane. Following the Lyapunov transformation of Equation 8, the radial and transversal components of the cartesian relative position vector in function of ROEs are:

$$\begin{cases} \delta x_R/a = \delta a - \delta e \sin(u - \varphi) \\ \delta x_T/a = \delta\lambda - \frac{3}{2}\delta a u + 2\delta e \sin(u - \varphi) \end{cases} \tag{16}$$

Within the hypotheses of the problem, the projection of the relative trajectory on the RN plane is constant: a specific ROE state identifies the $\mathcal{E}_{RN}$ ellipse. On the contrary, the curve obtained projecting the relative trajectory on the RT plane varies over time, due to the along-track drift caused by a non-vanishing relative semi-major axis. The representation depicted in Figure 2b is therefore only an instantaneous projection in RT of the relative trajectory. The ellipse shown will drift in the along-track direction T according to the value of δa. In the RT plane the dimensions of the ellipse can be easily computed, since the ellipse presents no rotation with respect to the RT axes. The semi-major and semi-minor axes of the RT projection ellipse depend only from the magnitude of the relative eccentricity vector, measuring $2\delta e$ and δe respectively. The use of minimum separations in the RT plane as a passive safety concept is therefore closely related to the sign and magnitude of the relative semi-major axis δa. In fact, the non-null energy difference between target and chaser orbit causes the RT projection of the trajectory to drift either away or in the direction of the target, at a speed proportional to the magnitude of δa. In this work, minimum separation on RT plan is used to impose ACS conditions, as for the final ROE state to be reached with a collision avoidance policy in the cases of off-nominal behaviour of the chaser during the approach. Therefore, a minimum separation in the RT plane is expressed by imposing a zero orbital energy difference between chaser and target. With this assumption, in order to keep the target within the ellipse of Figure 2b, the following relations must hold:

$$\begin{cases} \delta a = 0 \\ \delta\lambda \leq 2\delta e - R_{KOZ,RT} \\ -\delta\lambda \leq 2\delta e - R_{KOZ,RT} \\ \delta e \geq 2R_{KOZ,RT} \end{cases} \tag{17}$$

In the presence of a non-vanishing relative semi-major axis, Equations 17 can be employed by considering the ellipses translated in time along the T direction. Note that Equations 17 focus on the case when the target is kept within the projected ellipse. On the other hand, an extension of

the concept can be achieved by considering a separation, coupled with a drift direction, in order to ensure that the target remains outside the RT projected ellipse. This latter case has not been considered in this preliminary application of the ROE safety concept to forced motion to establish a post collision avoidance state, where the chaser remains in the vicinity of the target. As for the preliminary study addressed in this work, the two latter extensions of the safety policies in the RT plane are not investigated further.

ROE BASED GUIDANCE PROBLEM

The safety formulations introduced in the previous section are included in the problem of trajectory guidance in close-proximity of an uncooperative and non-collaborative target. Specifically, the forced motion to manoeuvre the chaser around a target within few tens of meters of separation is considered as a relevant application of the concept.

The close-range guidance problem treated in this work is cast as a constrained continuous time optimal control problem with fixed final time:

$$\min_{\mathbf{u}(t),\mathbf{u}^{ACS}(t)} \quad \int_{t_0}^{t_f} \mathcal{L}(t,\delta\boldsymbol{\alpha}(t),\mathbf{u}(t),\mathbf{u}^{ACS}(t))\mathrm{dt} \tag{18a}$$

$$\text{s.t.} \quad \dot{\delta\boldsymbol{\alpha}} = \mathrm{A}\delta\boldsymbol{\alpha} + \mathrm{B}(t)\mathbf{u}(t) \tag{18b}$$

$$\delta\boldsymbol{\alpha}(t_0) = \delta\boldsymbol{\alpha}_0 \tag{18c}$$

$$\delta\boldsymbol{\alpha}(t_f) = \delta\boldsymbol{\alpha}_f \tag{18d}$$

$$\mathcal{G}(t,\delta\boldsymbol{\alpha}(t),\mathbf{u}(t),\mathbf{u}^{ACS}(t)) \leq 0 \tag{18e}$$

$$\mathcal{H}(t,\delta\boldsymbol{\alpha}(t),\mathbf{u}(t),\mathbf{u}^{ACS}(t)) = 0 \tag{18f}$$

where Equation 18b convey the relative dynamics constraint, Equations 18c and 18d the initial and final boundary constraints, and Equations 18e and 18e the nonlinear inequality and equality path constraints used to impose the PAS and ACS conditions along the nominal trajectory. The cost function is represented by a Lagrangian contribution, dependent on the nominal states and controls along the nominal trajectory between initial and final time. An additional contribution of this work is to include in the Lagrangian cost function for the design of the nominal trajectory the cost of the collision avoidance policy $\mathbf{u}^{ACS}(t)$ together with the nominal states and nominal cost. This enables to design, within the guidance solution of the nominal trajectory, collision avoidance policies that do not result excessive use of control. The general formulation of Equation 18 is tailored to the proposed problem in this paper considering the following cost functions and constraints:

- **Cost function:** L1 norm cost considering both the nominal and the collision avoidance policy accelerations, which is strongly related to the fuel optimal cost for the trajectory:

$$\mathcal{L}(t,\delta\boldsymbol{\alpha}(t),\mathbf{u}(t),\mathbf{u}^{ACS}(t)) := \|\mathbf{u}(t)\|_1 + \lambda_{ACS}\|\mathbf{u}^{ACS}(t)\|_1$$

- **Path constraints:** PAS path constraints enforcing safety conditions expressed in function of ROE in Equation 14. ACS conditions by imposing RT minimum separation constraints of Equation 17 to the final state after the application of the collision avoidance policy and minimum 3D separation expressed by Equation 9 for the $\delta\boldsymbol{\alpha}^{ACS}(t)$ non-nominal states of collision policy application.

- **Control constraints:** Maximum acceleration U_{max} imposed for each direction in RTN with an L_∞ norm constraint on accelerations.

Discretizing in time the problem of Equation 18 and considering the accelerations constant in each interval, the nominal and non-nominal ROE dynamics can be expressed through Equation 6. Figure 3 depicts the dynamics discretization performed in the optimal control problem.

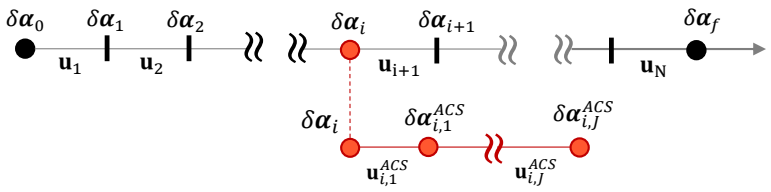

Figure 3: Discretisation of the controlled nominal ROE trajectory (black) and non-nominal collision policy application trajectory (red).

In this framework, the nominal state $\delta\alpha_i$ at time t_i can be expressed linearly in function of the piecewise constant accelerations applied previously and initial conditions as follows:

$$\delta\boldsymbol{\alpha}_i = \delta\boldsymbol{\alpha}(t_i) = \Phi(t_0, t_i)\delta\boldsymbol{\alpha}_0 + \begin{bmatrix}\Phi_{1,i}\Psi_{1,2} & \dots & \Phi_{1,i}\Psi_{i-1,i}\end{bmatrix} \begin{pmatrix}\mathbf{u}_1 \\ \vdots \\ \mathbf{u}_i\end{pmatrix} \tag{19}$$

Equation 19 can be conveniently reorganised by defining the following matrices and vectors:

$$\mathrm{G}_i = \begin{bmatrix}\Phi_{1,i}\Psi_{1,2} & \dots & \Phi_{1,i}\Psi_{i-1,i}\end{bmatrix}, \quad \mathrm{C}_i = \begin{bmatrix}\mathbb{I}_{(3i\times 3i)}, & 0_{(3\mathrm{i}\times 3(\mathrm{N}-\mathrm{i}))}\end{bmatrix}, \quad U = \begin{pmatrix}\mathbf{u}_1 \\ \vdots \\ \mathbf{u}_N\end{pmatrix} \tag{20}$$

where the C_i matrix composed by concatenation of the identity matrix $\mathbb{I}_{(i\times i)}$ of dimension $(3i \times 3i)$ and a zeros matrix $0_{(3\mathrm{i}\times 3(\mathrm{N}-\mathrm{i}))}$ of dimension $(3i \times 3(N-i))$ serves to the purpose of selecting the accelerations up to the node i from the full vector of acceleration U. This enables to enforce the dynamics and final boundary constraints to be enforced with the following linear equality relation:

$$\delta\boldsymbol{\alpha}_f = \Phi(t_0, t_i)\delta\boldsymbol{\alpha}_0 + \mathrm{H}_f U \quad \text{with} \quad \mathrm{H}_f = \mathrm{G}_f\mathrm{C}_f \tag{21}$$

The cost function of Equation 18a is then expressed as:

$$J_m := \sum_{i=1}^{N} \|\mathbf{u}_i\|_1 + \lambda_{ACS} \sum_{m}^{M} \sum_{j=1}^{J} \|\mathbf{u}_{m,j}^{ACS}\|_1 \tag{22}$$

where also for the discretisation in J nodes of each segment of non-nominal trajectory stemming from each of the M nominal ACS constraints nodes is included, see Figure 3. The cumulated cost of the collision avoidance policies is weighted with λ_{ACS} with respect to the nominal trajectory cost. The path constraints can then be formulated imposing the PAS and ACS nonlinear safety conditions to the nominal states $\delta\boldsymbol{\alpha}_i$ and $\delta\boldsymbol{\alpha}_{m,j}^{ACS}$ at each constrained node, expressed by Equation 19.

Sequential convex programming

Referring to the optimal control guidance problem of Equation 18, the constraints conveying both the relative dynamics and of the boundary conditions are linear equations in the problem's variables. Nonetheless, as an whole, it is still a Nonlinear Programming Problem (NLP) due to the structure of the safety path constraints. Indeed, the safety constraints introduced in the previous section contained in the $\mathcal{F}(\cdot)$ and $\mathcal{G}(\cdot)$ functions represent a non-convex constraints to be enforced. In this work the NLP is solved exploiting a sequential convex programming method, which iteratively solves a convex sub-problem built to approximate the original NLP until the cost minimisation reaches convergence.[23–25] In the formulation of the convex (specifically linear) subproblem, firstly the infinity norm maximum accelerations are simplified as follows:

$$\|\mathbf{u}_i\|_\infty \leq U_{max} \tag{23}$$

$$\overline{\mathbf{u}} = \begin{pmatrix} \mathbf{u}^+ \\ \mathbf{u}^- \end{pmatrix}, \quad \mathbf{u} = \mathbf{u}^+ - \mathbf{u}^-, \quad \overline{\mathbf{u}} \leq U_{max} \tag{24}$$

where the accelerations are augmented considering auxiliary variables $\mathbf{u}^-$ and $\mathbf{u}^+$ to render the control constraints linear by imposing the components of $\overline{\mathbf{u}}$ strictly positive and bounded by U_{max}. The cost function of Equation 22 is written in a linear form:

$$J_m = \boldsymbol{f}^T \overline{U} + \boldsymbol{f}_{ACS}^T \overline{U}^{ACS} \tag{25}$$

where $\boldsymbol{f}$ and $\boldsymbol{f}_{ACS}$ are vectors of ones of dimension respectively $(3N \times 1)$ and $(3MJ \times 1)$. Concerning the handling of the PAS and ACS non-linear constraints, within the SCP technique they are linearised locally around a reference solution. More in details, the reference solution is taken at each iteration of the SCP as the previous iteration solution $\delta\boldsymbol{\alpha}^{k-1}$.

The convex sub-problem is then written as:

$$\min_{\overline{U}_i^k, \overline{U}^{ACS,k}, \nu_p^k, \nu_q^k} \quad \boldsymbol{f}^T \overline{U} + \boldsymbol{f}_{ACS}^T \overline{U}^{ACS} + \lambda_{slack} \left(\sum_q^Q \boldsymbol{\nu}_q^k + \sum_p^P \boldsymbol{\nu}_p^k \right) \tag{26a}$$

$$\text{s.t.} \quad \delta\boldsymbol{\alpha}_f = \Phi(t_0, t_i)\delta\boldsymbol{\alpha}_0 + \mathrm{H}_f U^k \tag{26b}$$

$$\delta\boldsymbol{\alpha}(t_0) = \delta\boldsymbol{\alpha}_0 \tag{26c}$$

$$\mathcal{G}(\delta\alpha^{k-1}, \mathbf{u}^{k-1}) + \nabla^{\mathrm{T}}\mathcal{G}^{k-1} \left(\delta\alpha^k - \delta\alpha^{k-1} \right) \leq \nu_p^k \tag{26d}$$

$$\mathcal{H}(\delta\alpha^{k-1}, \mathbf{u}^{k-1}) + \nabla^{\mathrm{T}}\mathcal{H}^{k-1} \left(\delta\alpha^k - \delta\alpha^{k-1} \right) = \nu_q^k \tag{26e}$$

$$|\delta\alpha^k - \delta\alpha^{k-1}| \leq \rho^k \tag{26f}$$

$$\nu_p \geq 0 \tag{26g}$$

$$\nu_q \geq 0 \tag{26h}$$

where the matrices $\nabla^{\mathrm{T}}\mathcal{G}^{k-1}$ and $\nabla^{\mathrm{T}}\mathcal{H}^{k-1}$ represent the gradient of the constraint functions evaluated at the previous iteration solution $\delta\boldsymbol{\alpha}^{k-1}$. The variables ν_p and ν_q are included as slack variables to relax the constraints' enforcement during the iterations. Moreover, a hard-trust region method conveyed by Equation 26f is added to maintain the solution at each iteration within region of the state space where the linearisation of the non-convex functions is considered reliable.[24] The trust region radius ρ_k is adapted during iterations according to the method of relative decrease described

in the work of Reynolds et al.,[24] and omitted here for the sake of brevity. The sub-problem of Equation 26 is reduced to a Linear Program (LP), which can be efficiently solved with robust numerical techniques such as simplex or interior point based algorithms.

RESULTS AND DISCUSSION

In this section the results of two test cases for the safe guidance algorithm developed are presented. Test case A describes a reconfiguration between two relative orbits with null semi-major axis difference and characterized by E/I vector separation. While, test case B is defined as a synchronisation of the chaser trajectory to a rotating hold point motion around the target with a predefined angular rate ω_{hp} and constant separation d_{hp}. The latter scenario is defined to mimic a full/partial synchronisation to the target tumbling motion and to evaluate the safety concepts defined in this work during this challenging scenario. The algorithms are implemented in Matlab® and the linear sub-problems of the SCP iterations are solved with the dual-simplex algorithm.

Passive relative orbit reconfiguration

Initial and final conditions for test case A are defined considering a change of geometry of two passively safe relative orbits around the target. In particular, a zero relative semi-major axis and E/I separation are set for the initial and final boundary conditions. The PAS constraints are enforced along the whole reconfiguration controlled trajectory and a fixed reconfiguration time is set equal to one orbital period. The solution of the guidance problem using the SCP method is obtained considering two formulations PAS for comparison. The novel formulations in terms of ROEs introduced in this work is compared with PAS constraints enforcing Equation 9 to a future discretization of the uncontrolled trajectory stemming from the nominal nodes. The two problems are referred as PAS-ROE and PAS-CAR respectively and they are both solved with the SCP method. In the PAS-CAR the uncontrolled trajectory after the PAS nodes is propagated for a ΔT time interval and the constraint of Equation 9 enforced at M nodes along this time interval, as performed in previous work for example in Breger et al.[6] The aforementioned time interval ΔT is considered equal to one orbital period throughout this work. The ROE based PAS constraints of Equation 14 are capable of ensuring PAS imposing solely two conditions on the nominal nodes, hence resulting in a number of constraints on the trajectory of $2N$. On the other hand, in the PAS-CAR case, considering a discretisation of M nodes for each uncontrolled interval stemming from the nominal N nodes, the total number of constraints will be $N \times M$. The parameters and boundary conditions for test case A are shown in Table 1.

Table 1: Boundary conditions and parameters of test case A.

Initial condition	$a\delta\boldsymbol{\alpha}_0$	$[0, 0, 0, 100, 0, 100]^{\mathrm{T}}$ m	**Final time**	T_f	1 Period
Final condition	$a\delta\boldsymbol{\alpha}_f$	$[0, 0, 15.36, -4.47, 15.36, 4.47]^{\mathrm{T}}$ m	**Orbit period**	T	5801 s
Nodes	N	150	**PAS nodes**	N_{PAS}	150
ACS nodes	N_{ACS}	none	**KOZ radius**	R_{KOZ}	12 m
			Max accel.	U_{max}	1e-4 $\mathrm{m/s^2}$

The trajectory solutions of the SCP based algorithms developed in this work for test case A are shown in Figure 4, where the PAS-CAR trajectory is computed considering $M = 20$ nodes of PAS checks in the uncontrolled trajectory propagation from the target. The control acceleration histories shown in Figure 5 show the expected bang-bang control structure consequence of a L1 norm based

cost function. Additionally as shown in the plots, the PAS-CAR trajectory only slightly differs from the fuel optimal unconstrained case, while the PAS-ROE shows more discrepancy due to the stronger PAS condition embodied in the ROE based approach. In fact, in the PAS-CAR problem the constraints guarantee the avoidance of the KOZ only for the enforced ΔT time of one period. It is however possible that due to δa-induced drift the condition is violated after the ΔT time under natural Keplerian relative dynamics.

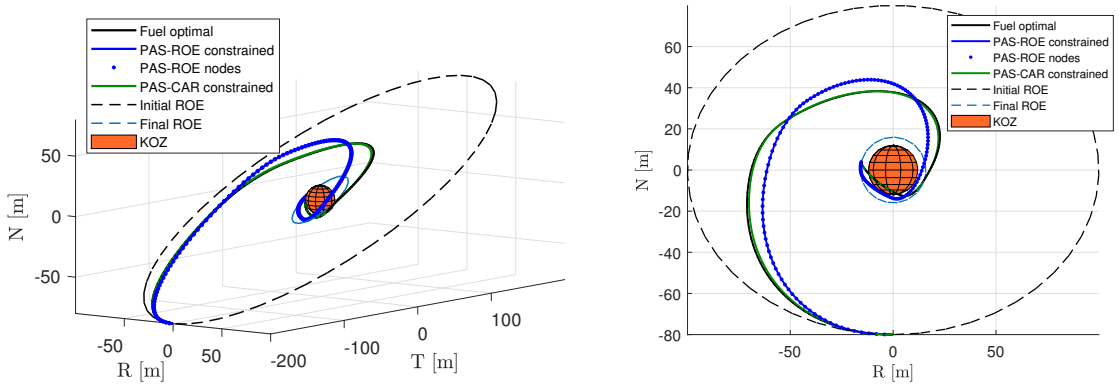

Figure 4: Forced motion trajectories for test case A obtained considering the SCP guidance algorithms developed.

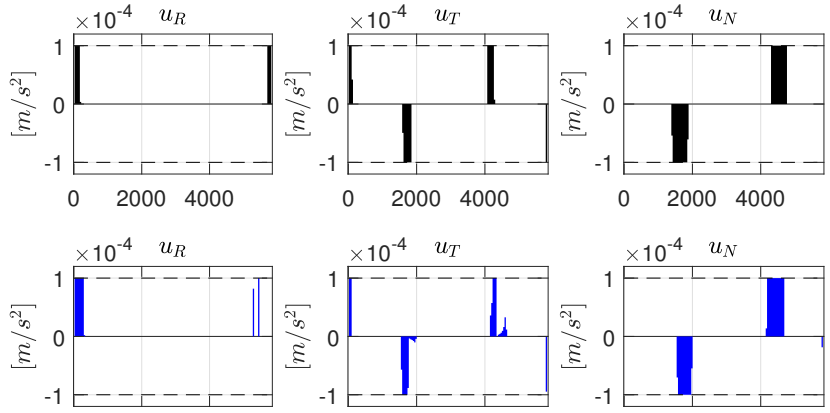

Figure 5: Control accelerations for test case 1 for the fuel optimal solution (black) and PAS-ROE solution constrained trajectory (blue). The solution referred as PAS-CAR is not plotted, being basically coincident with the fuel optimal case.

Figure 6 shows the projection of the ROE state ellipse onto the RN plane using the ROE state at each PAS node for the fuel optimal and PAS-ROE cases, demonstrating the capability of the developed safe guidance algorithm to satisfy the predefined minimum safety distance from the KOZ around the target. Figure 7 shows instead the future uncontrolled evolution of the guidance trajectory in the PAS-CAR solution for each of the enforced PAS node. As it can be noted more clearly from Figure 6, the PAS-CAR (as for the fuel optimal case) do not guarantee the passive safety as minimum separation in the RN plane.

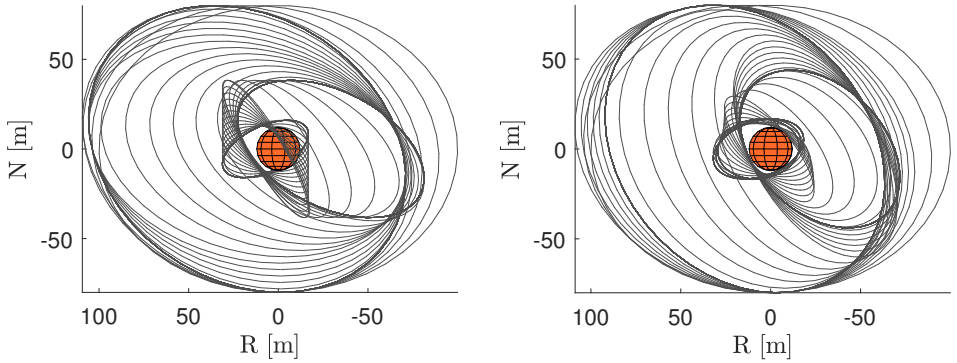

Figure 6: Projection of the relative trajectory related to the ROE states of PAS nodes for test case 1. The solution of fuel optimal algorithm (left) and PAS-ROE algorithm (right) are displayed.

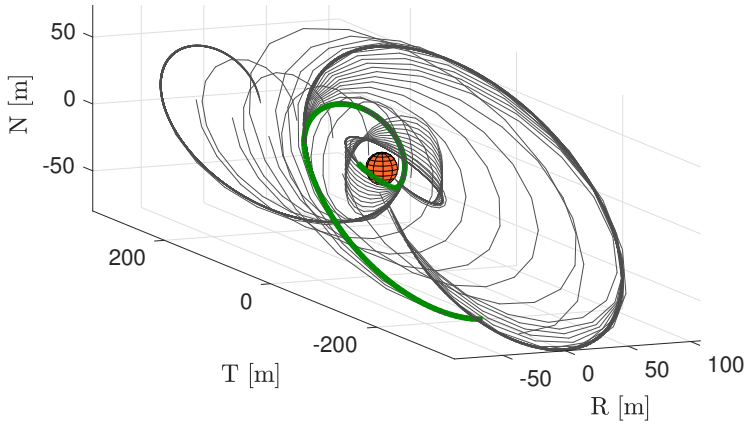

Figure 7: Uncontrolled relative trajectories propagated from each of the PAS nodes for 1 orbital period for the PAS-CAR case with M = 20. The nominal trajectory is shown in green.

Table 2: Performances of the safe guidance SCP algorithms for test case A.

Solution	$\delta\mathbf{v_{tot}}$ **[m/s]**	**CPU time [s]**	**Iterations**
Fuel optimal	0.1798	0.04	N/A
PAS-ROE	0.18281	0.4788	4
PAS-CAR (M=10)	0.17978	0.8903	3
PAS-CAR (M=20)	0.17979	1.4742	3
PAS-CAR (M=50)	0.17980	3.7939	3
PAS-CAR (M=100)	0.17980	8.5201	3

The more robust safety provided by the G-PAS-ROE solution comes at the cost of a slightly larger delta-v expense as compared against the fuel-optimal and G-PAS-CAR solutions (see δv_{tot} cost in Table 2). Additionally, Table 2 highlights the computational expense of increasing the number of nodes in the transcription of the passive abort condition for the PAS-CAR case. Note that the CPU time reported refers only to the time taken to solve each convex sub-problem for the different cases. The results demonstrate that introducing PAS condition in terms of ROE both improves the safety robustness and the efficiency of the transcription by reducing the number of constraints required. The latter feature is particularly useful since removes the scalability of the

problem size and constraints to be enforced with respect to the future ΔT time and to the number of PAS checks. It is worth remarking that generally in the PAS-ROE case the number of iterations of the trust-region-like SCP algorithm are greater than the PAS-CAR due to the slightly more severe non-convexity introduced by the ROE based constraints.

Hold point synchronisation

Test case B is a scenario of synchronisation of the chaser to a rotating hold point around the target. The hold point motion is defined considering a circular motion around the target at a constant distance d_{hp} and on a fixed plane in RTN. The definition of the present test case aims at evaluating how safety constraints based on ROE behave in a more demanding scenario in terms of energy of the forced motion trajectory. In fact, the final boundary condition of the scenario that fixes both position and velocity of the final state, strongly reduces the feasible space to enforce the PAS condition based on ROE in the last section of the trajectory. For this type of demanding scenarios the definition introduced in this paper of active collision avoidance safety becomes extremely useful. In fact, in the last part of the trajectory the safety considerations are enforced as ACS constraints imposing a minimum separation on the RT plane based on ROE conditions according to Equation 17 after a time ΔT_{ACS} of application of the collision avoidance policy. As explained in the previous section, the ACS policy is included in the cost function of the guidance problem with a penalty factor to avoid the use of excessive control authority in the collision avoidance manoeuvres. By enforcing the separation on RT of the final ACS node, the ACS accelerations present only the in-plane components thus reducing the dimensionality of the $\overline{U}^{ACS}$ vector in the design of the SCP algorithm. Additionally, during the application of the collision avoidance manoeuvres over ΔT_{ACS} time interval the minimum separation in Cartesian coordinates according to Equation 9 is also imposed. Here the three-dimensional definition of minimum separation is used instead of RN or RT separations to allow more freedom in the motion of the chaser to reach the final target collision avoidance state. A stricter conditions in the RT and RN plane may render the final collision avoidance state not reachable starting from the initial ACS node on the nominal trajectory. The test case B scenario and parameters are reported in Table 3.

Table 3: Parameters and conditions for test case B.

Boundary Conditions		
Initial ROE	$a\delta\boldsymbol{\alpha}_0$	[0,0,0,100,0,100] m
Final ROE	$a\delta\boldsymbol{\alpha}_f$	[-233.6,-108.1,-221.5,49.6,6.6,-0.6] m
Final time	T_f	1 period
Orbit period	T	5801 s
Hold point angular rate	ω_{hp}	0.5 deg/s
Hold point distance	d_{hp}	15 m

Parameters					
Max acceleration	U_{max}	2e-4 m/s^2	**Nodes**	N	150
KOZ radius	R_{KOZ}	12 m	**PAS nodes**	N_{PAS}	112
ACS policy max acceleration	U_{max}^{ACS}	4e-4 m/s^2	**ACS nodes**	N_{ACS}	38
ACS policy nodes	J	3	**ACS penalty**	λ_{ACS}	1e-3
ACS policy duration	ΔT_{ACS}	600 s			

In Figure 8a and Figure 8b the trajectories in RTN and the control accelerations are shown for the fuel optimal and the safety constrained solutions. As expected, the safety constraints strongly affect the trajectory of the chaser, which is required to avoid ROE states that do not guarantee PAS in the first section. As a result, also the ACS section of the trajectory displayed in red in Figure 8a is different than the fuel optimal case.

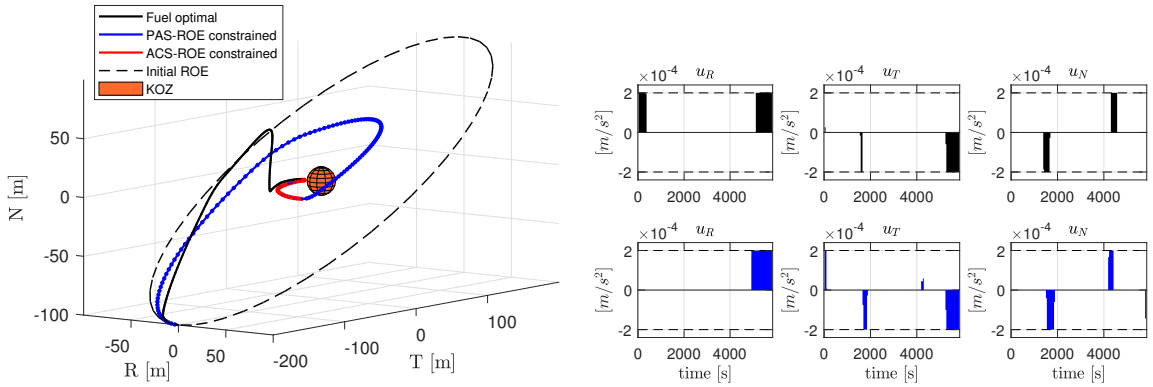

(a) (b)

Figure 8: (a) Trajectories in RTN of the fuel optimal and safety constrained case of test case B. In blue and red are respectively the PAS and ACS section of the safety constrained solution, while the fuel optimal solution is displayed in black.(b) Control acceleration for fuel optimal (black) and safety constrained solution (blue).

In Figure 9 the RN projection of the future uncontrolled trajectories related to the ROE state of PAS constrained nodes are shown for the fuel optimal and safety constraints solution. It can be seen how the SCP algorithm is capable of imposing the minimum RN separation by the ROE based constraints, otherwise violated in the fuel optimal solution in the first section of trajectory. It is worth remarking here how the trajectory with passive safety uses the regions of the ROE space with non-null semi-major axis and non-parallel relative eccentricity and inclination vectors. Indeed, this proves the generalization to the classical E/I based passive safety. The RN projection of the relative trajectory is an ellipse with both rotation and translation with respect to the RN axes. Table 4 shows that the implemented safe guidance algorithms is capable to provide a solution with both computational efficiency and delta-v cost comparable to the fuel-optimal solution, even in the extremely demanding operational scenario of test case B. At the same time, the actual close-range trajectory in RTN of the safe solution is drastically different than the fuel optimal one: it provides a higher level of safety. In Figure 10 the RT projections related to the uncontrolled trajectory of the last node of ACS time intervals are shown. The algorithm is capable of maintaining the required RT separation after the designed collision avoidance policy for non-nominal operation for every ACS node. The in-plane accelerations related to the collision avoidance policy $\mathbf{u}^{ACS}$ in each of the $M \times J$ node of the non-nominal controlled trajectory are also shown.

Table 4: Performances of the safe guidance SCP algorithm for test case B.

Solution	$\delta \mathbf{v_{tot}}$ [m/s]	CPU time [s]	Iterations
Fuel optimal	0.448	0.001	N/A
PAS-ROE	0.466	1.08	8

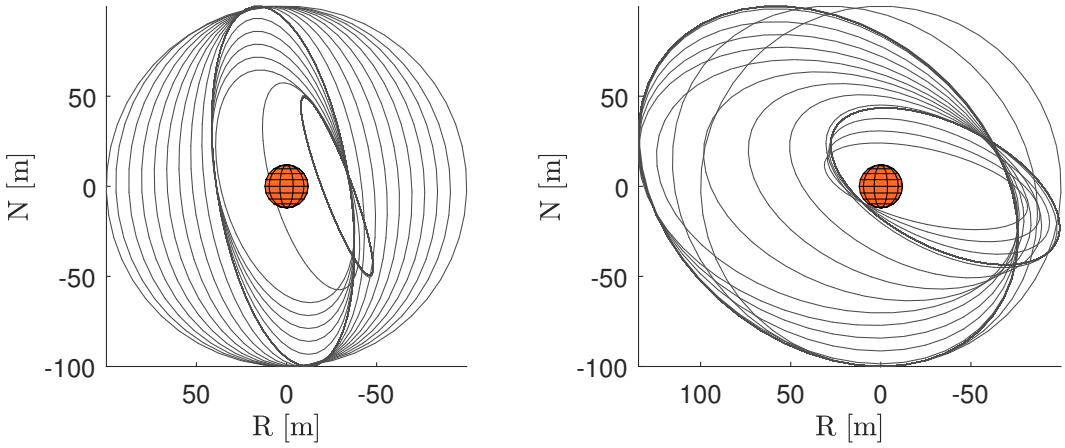

Figure 9: RN projection of the future uncontrolled trajectories correspondent to the ROE of PAS constrained nodes for test case B. The fuel optimal solution (left) and the safety constrained solution (right) are reported.

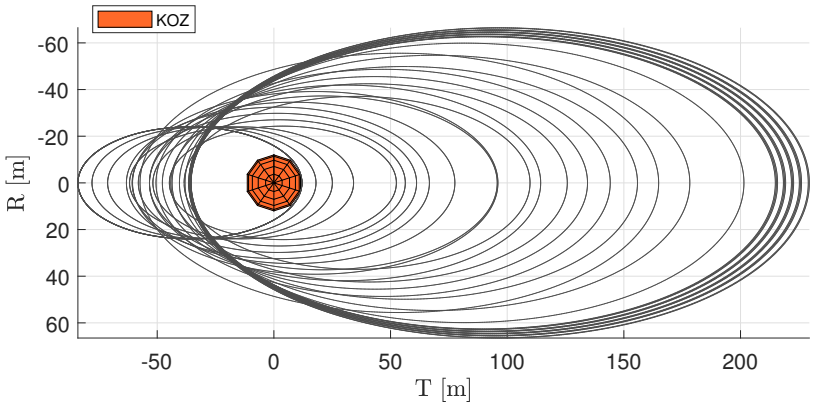

Figure 10: Projection in the RT plane of the trajectories obtained by the guidance algorithms after the application of the collision avoidance policy after each ACS node.

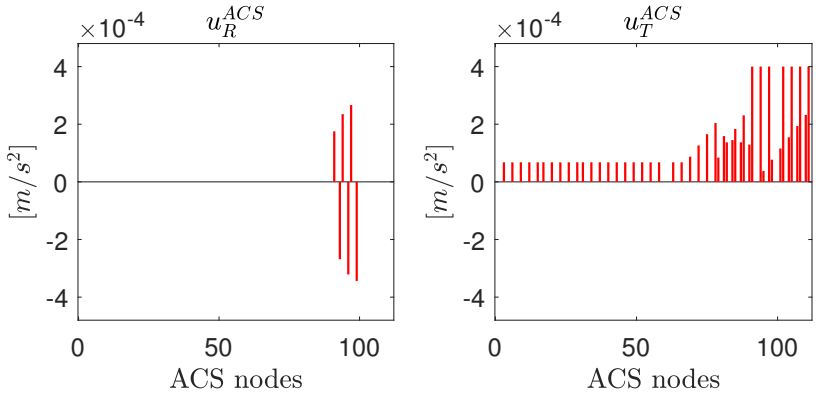

Figure 11: In-plane acceleration of the collision avoidance policy non-nominal segment for all the M ACS nodes.

CONCLUSIONS

This work proposes new formulations of safety concepts applicable to demanding proximity operations scenarios. The forced motion trajectory design within separation of few tens of meters are considered to apply such safety concepts aimed to extend passive abort and active collision avoidance safety formulations in the relative orbital element framework. The proximity guidance solution for two test cases is solved efficiently with a sequential convex programming scheme that allows the computation of a feasible optimal solution with limited computational expenses. The work demonstrated that for the scenarios studied the novel relative orbital elements based safety formulations improve the classical Cartesian keep out constraints check both in terms of number of constraints enforced and robustness of safety guaranteed.

ACKNOWLEDGEMENT

The research leading to these results has received funding from the European Research Council (ERC) under the European Union's Horizon2020 research and innovation programme as part of project COMPASS (Grant agreement No 679086). The contribution of Dr. Gabriella Gaias is funded by the European Union's Horizon 2020 research and innovation programme under the Marie-Sklodowoska Curie grant ReMoVE (grant agreement nr 793361).

REFERENCES

[1] I. Kawano, M. Mokuno, T. Kasai, and T. Suzuki, "Result of Autonomous Rendezvous Docking Experiment of Engineering Test Satellite-VII," *Journal of Spacecraft and Rockets*, Vol. 38, No. 1, 2001, pp. 105–111, 10.2514/2.3661.

[2] "Overview of the DART Mishap Investigation Results For Public Release, `http://www.nasa.gov/pdf/148072main_DART_mishap_overview.pdf`," Accessed: 2022-08-24.

[3] "`https://astroscale.com/astroscales-elsa-d-mission-successfully-completes-complex-rendezvous-operation/`," Accessed: 2022-08-24.

[4] G. Boyarko, O. Yakimenko, and M. Romano, "Optimal Rendezvous Trajectories of a Controlled Spacecraft and a Tumbling Object," *Journal of Guidance, Control, and Dynamics*, Vol. 34, No. 4, 2011, pp. 1239–1252, 10.2514/1.47645.

[5] G. Gaias and M. Lovera, "Safe Trajectory Design for Close Proximity Operations," *Advances in the Astronautical Sciences*, Vol. 175, 2021, pp. 4015–4029.

[6] L. Breger and J. P. How, "Safe trajectories for autonomous rendezvous of spacecraft," *Journal of Guidance, Control, and Dynamics*, Vol. 31, No. 5, 2008, pp. 1478–1489, 10.2514/1.29590.

[7] D. Morgan, S.-J. Chung, and F. Y. Hadaegh, "Model Predictive Control of Swarms of Spacecraft Using Sequential Convex Programming," *Journal of Guidance, Control, and Dynamics*, Vol. 37, No. 6, 2014, pp. 1725–1740, 10.2514/1.G000218.

[8] P. Lu and X. Liu, "Autonomous Trajectory Planning for Rendezvous and Proximity Operations by Conic Optimization," *Journal of Guidance, Control, and Dynamics*, Vol. 36, No. 2, 2013, pp. 375–389, 10.2514/1.58436.

[9] F. Scala, G. Gaias, C. Colombo, and M. Martín-Neira, "Design of optimal low-thrust manoeuvres for remote sensing multi-satellite formation flying in low Earth orbit," *Advances in Space Research*, Vol. 68, No. 11, 2021, pp. 4359–4378, https://doi.org/10.1016/j.asr.2021.09.030.

[10] J. Liu and H. Li, "Artificial Potential Function Safety and Obstacle Avoidance Guidance for Autonomous Rendezvous and Docking with Noncooperative Target," *Mathematical Problems in Engineering*, Vol. 2019, Aug 2019, p. 3451864, 10.1155/2019/3451864.

[11] R. Bevilacqua, T. Lehmann, and M. Romano, "Development and experimentation of LQR/APF guidance and control for autonomous proximity maneuvers of multiple spacecraft," *Acta Astronautica*, Vol. 68, No. 7, 2011, pp. 1260–1275, https://doi.org/10.1016/j.actaastro.2010.08.012.

[12] I. Lopez and C. R. Mclnnes, "Autonomous rendezvous using artificial potential function guidance," *Journal of Guidance, Control, and Dynamics*, Vol. 18, No. 2, 1995, pp. 237–241, 10.2514/3.21375.

[13] S. D'Amico and O. Montenbruck, "Proximity Operations of Formation-Flying Spacecraft Using an Eccentricity/Inclination Vector Separation," *Journal of Guidance, Control, and Dynamics*, Vol. 29, No. 3, 2006, pp. 554–563, 10.2514/1.15114.

[14] S. D'Amico, J.-S. Ardaens, G. Gaias, H. Benninghoff, B. Schlepp, and J. L. Jørgensen, "Noncooperative Rendezvous Using Angles-Only Optical Navigation: System Design and Flight Results," *Journal of Guidance, Control, and Dynamics*, Vol. 36, No. 6, 2013, pp. 1576–1595, 10.2514/1.59236.

[15] G. Gaias and J.-S. Ardaens, "Flight demonstration of autonomous noncooperative rendezvous in low earth orbit," *Journal of Guidance, Control, and Dynamics*, Vol. 41, No. 6, 2018, pp. 1337–1354.

[16] G. Gaias and J.-S. Ardaens, "Design challenges and safety concept for the AVANTI experiment," *Acta Astronautica*, Vol. 123, 2016, pp. 409–419. Special Section: Selected Papers from the International Workshop on Satellite Constellations and Formation Flying 2015, https://doi.org/10.1016/j.actaastro.2015.12.034.

[17] S. D'Amico, *Autonomous formation flying in low earth orbit*. PhD thesis, TU Delft, 2010.

[18] G. Gaias and M. Lovera, "Trajectory Design for Proximity Operations: The Relative Orbital Elements' Perspective," *Journal of Guidance, Control, and Dynamics*, Vol. 44, No. 12, 2021, pp. 2294–2302, 10.2514/1.G006175.

[19] G. Borelli, G. Gaias, and C. Colombo, "Rendezvous and Proximity Operations Design of an Active Debris Removal Service to a Large Constellation Fleet," 2021.

[20] M. Vavrina, C. Skelton, K. Deweese, B. Naasz, D. Gaylor, and C. D'souza, "Safe rendezvous trajectory design for the restore-l mission," Advances in the Astronautical Sciences, 2019, pp. 3649–3668.

[21] ESA CDF Team, "e.Inspector CDF Study Report - Assessment of an ENVISAT Imaging Mission as a Precursor to a Potential ENVISAT Deorbit," tech. rep., European Space Agency (ESA), 2017.

[22] S. Silvestrini, J. Prinetto, G. Zanotti, and M. Lavagna, "Design of Robust Passively Safe Relative Trajectories for Uncooperative Debris Imaging in Preparation to Removal," Vol. 175, 2021, p. 4205 – 4222.

[23] Y. Mao, D. Dueri, M. Szmuk, and B. Açıkmeşe, "Successive Convexification of Non-Convex Optimal Control Problems with State Constraints," *IFAC-PapersOnLine*, Vol. 50, No. 1, 2017, pp. 4063–4069. 20th IFAC World Congress, https://doi.org/10.1016/j.ifacol.2017.08.789.

[24] T. P. Reynolds and M. Mesbahi, "The Crawling Phenomenon in Sequential Convex Programming," *2020 American Control Conference (ACC)*, 2020, pp. 3613–3618, 10.23919/ACC45564.2020.9147550.

[25] R. Bonalli, A. Cauligi, A. Bylard, and M. Pavone, "GuSTO: Guaranteed Sequential Trajectory Optimization via Sequential Convex Programming," 2019, 10.48550/ARXIV.1903.00155.